SUPPLEMENTAL INFORMATION

Maintenance of metabolic homeostasis by Sestrin 2 and 3

Jun Hee Lee, Andrei V. Budanov, Saswata Talukdar, Eek Joong Park, Hae Li Park, Hwan-Woo Park, Gautam Bandyopadhyay, Ning Li, Mariam Aghajan, Insook Jang, Amber M. Wolfe, Guy A. Perkins, Mark H. Ellisman, Ethan Bier, Miriam Scadeng, Marc Foretz, Benoit Viollet, Jerrold Olefsky, Michael Karin

INVENTORY OF SUPPLEMENTAL INFORMATION

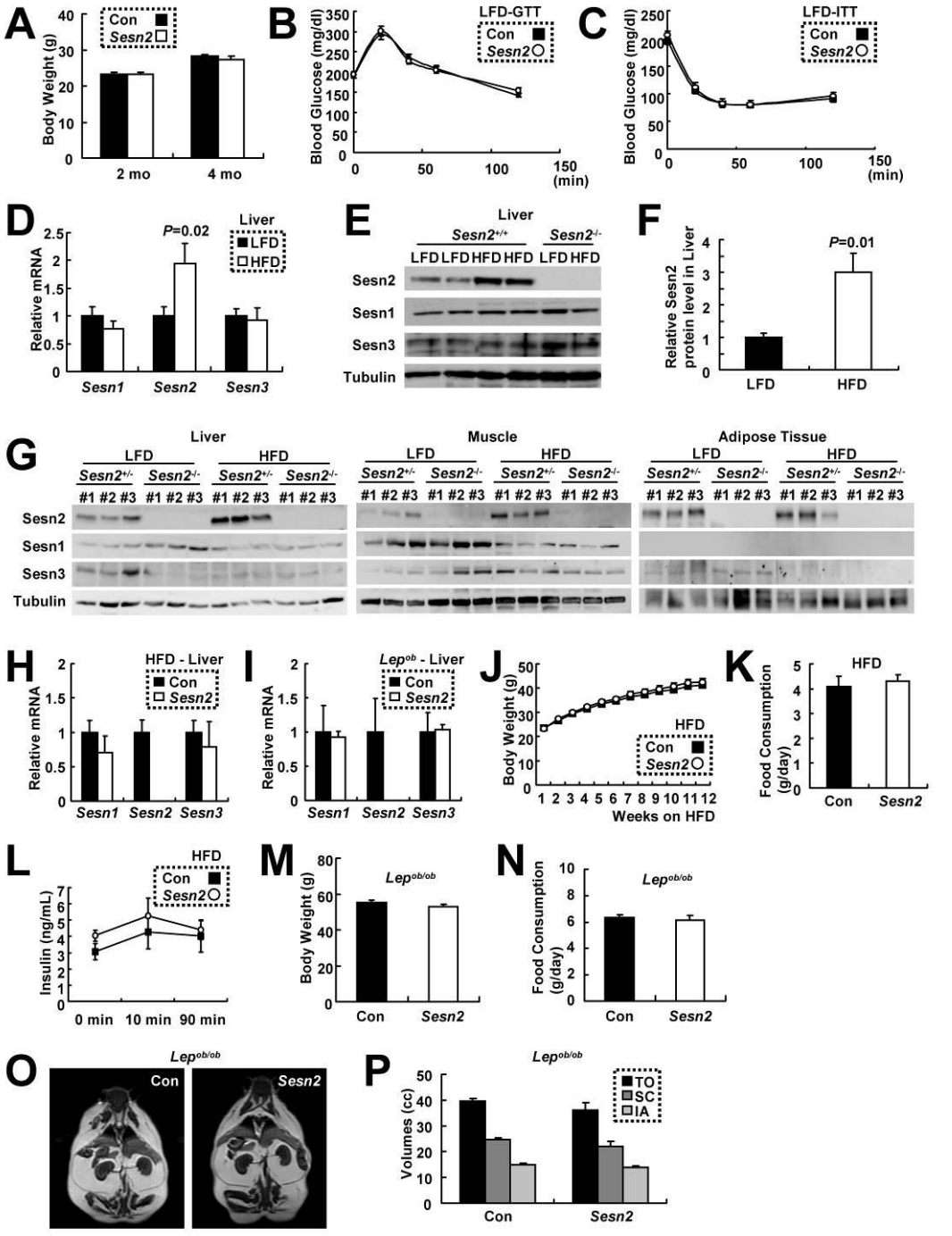
A
Body Weight (g)
Con
Sesn2
2 mo
4 mo
B
LFD-GTT
Blood Glucose (mg/dl)
Con
Sesn2
(min)
C
LFD-ITT
Blood Glucose (mg/dl)
Con
Sesn2
(min)
D
Liver
P=0.02
LFD
HFD
Relative mRNA
Sesn1
Sesn2
Sesn3
E
Liver
Sesn2+/+
Sesn2-/-
LFD LFD HFD HFD LFD HFD
Sesn2
Sesn1
Sesn3
Tubulin
F
P=0.01
Relative Sesn2 protein level in Liver
LFD
HFD
G
Liver
Muscle
Adipose Tissue
LFD
HFD
Sesn2+/-
Sesn2-/-
#1 #2 #3
Sesn2
Sesn1
Sesn3
Tubulin
H
HFD - Liver
Con
Sesn2
Relative mRNA
Sesn1 Sesn2 Sesn3
I
Lepob - Liver
Con
Sesn2
Relative mRNA
Sesn1 Sesn2 Sesn3
J
Body Weight (g)
HFD
Con
Sesn2
Weeks on HFD
K
HFD
Food Consumption (g/day)
Con
Sesn2
L
HFD
Con
Sesn2
Insulin (ng/mL)
0 min 10 min 90 min
M
Lepob/ob
Body Weight (g)
Con
Sesn2
N
Lepob/ob
Food Consumption (g/day)
Con
Sesn2
O
Lepob/ob
Con
Sesn2
P
Lepob/ob
TO
SC
IA
Volumes (cc)
Con
Sesn2

Figure S1

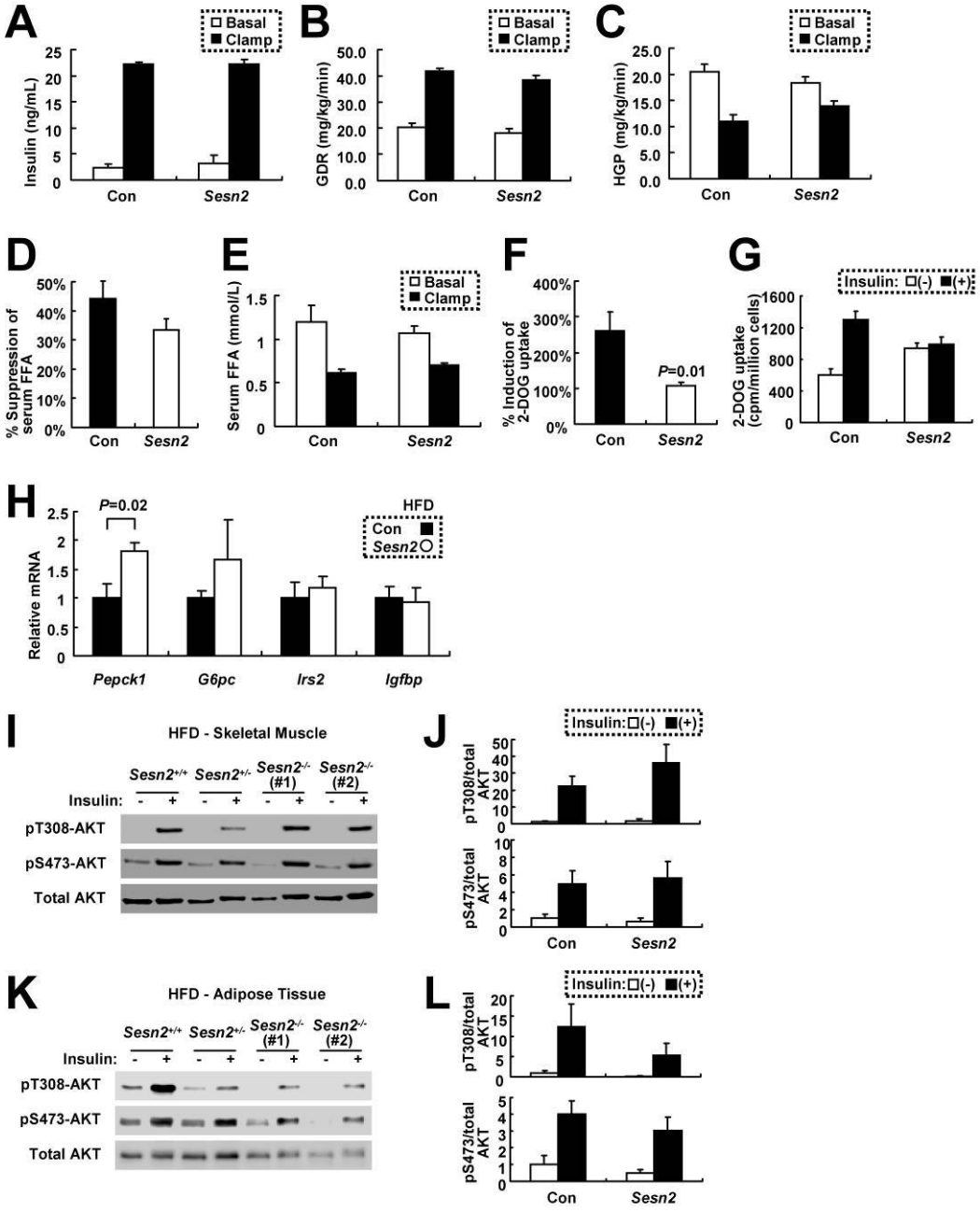
A
Basal
Clamp
Insulin (ng/mL)
Con
Sesn2
B
GDR (mg/kg/min)
C
HGP (mg/kg/min)
D
% Suppression of serum FFA
E
Serum FFA (mmol/L)
F
% Induction of 2-DOG uptake
P=0.01
G
Insulin: □(-) ■(+)
2-DOG uptake (cpm/million cells)
H
P=0.02
HFD
Con
Sesn2
Relative mRNA
Pepck1
G6pc
Irs2
Igfbp
I
HFD - Skeletal Muscle
Sesn2+/+
Sesn2+/-
Sesn2-/- (#1)
Sesn2-/- (#2)
Insulin:
pT308-AKT
pS473-AKT
Total AKT
J
pT308/total AKT
pS473/total AKT
K
HFD - Adipose Tissue
L

Figure S2

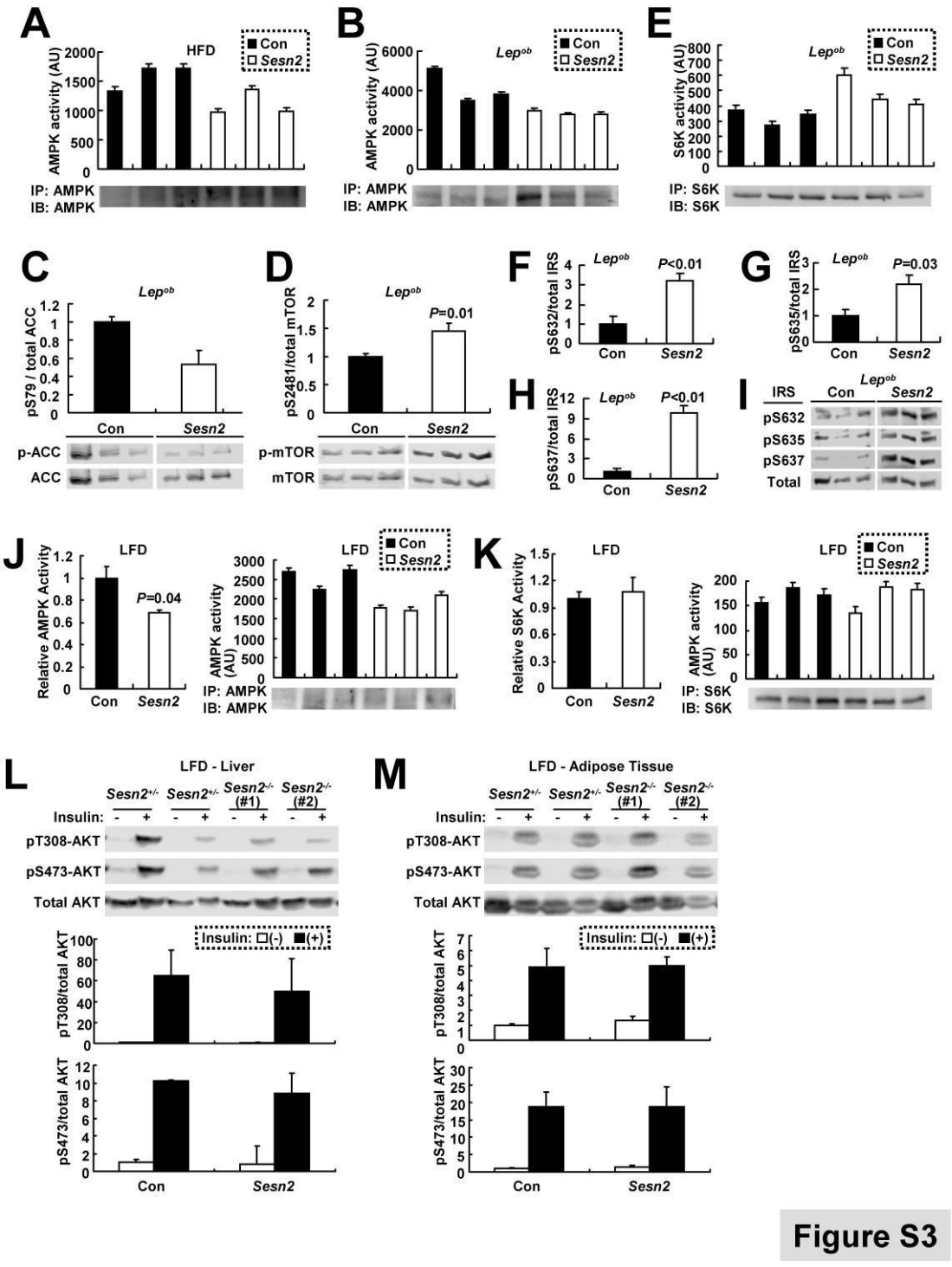
A
HFD
Con
Sesn2
AMPK activity (AU)
IP: AMPK
IB: AMPK
B
Lepob
C
pS79 / total ACC
p-ACC
ACC
D
pS2481/total mTOR
P=0.01
p-mTOR
mTOR
E
S6K activity (AU)
IP: S6K
IB: S6K
F
pS632/total IRS
P<0.01
G
pS635/total IRS
P=0.03
H
pS637/total IRS
I
IRS
pS632
pS635
pS637
Total
J
LFD
Relative AMPK Activity
P=0.04
K
Relative S6K Activity
L
LFD - Liver
Insulin:
pT308-AKT
pS473-AKT
Total AKT
pT308/total AKT
pS473/total AKT
M
LFD - Adipose Tissue

Figure S3

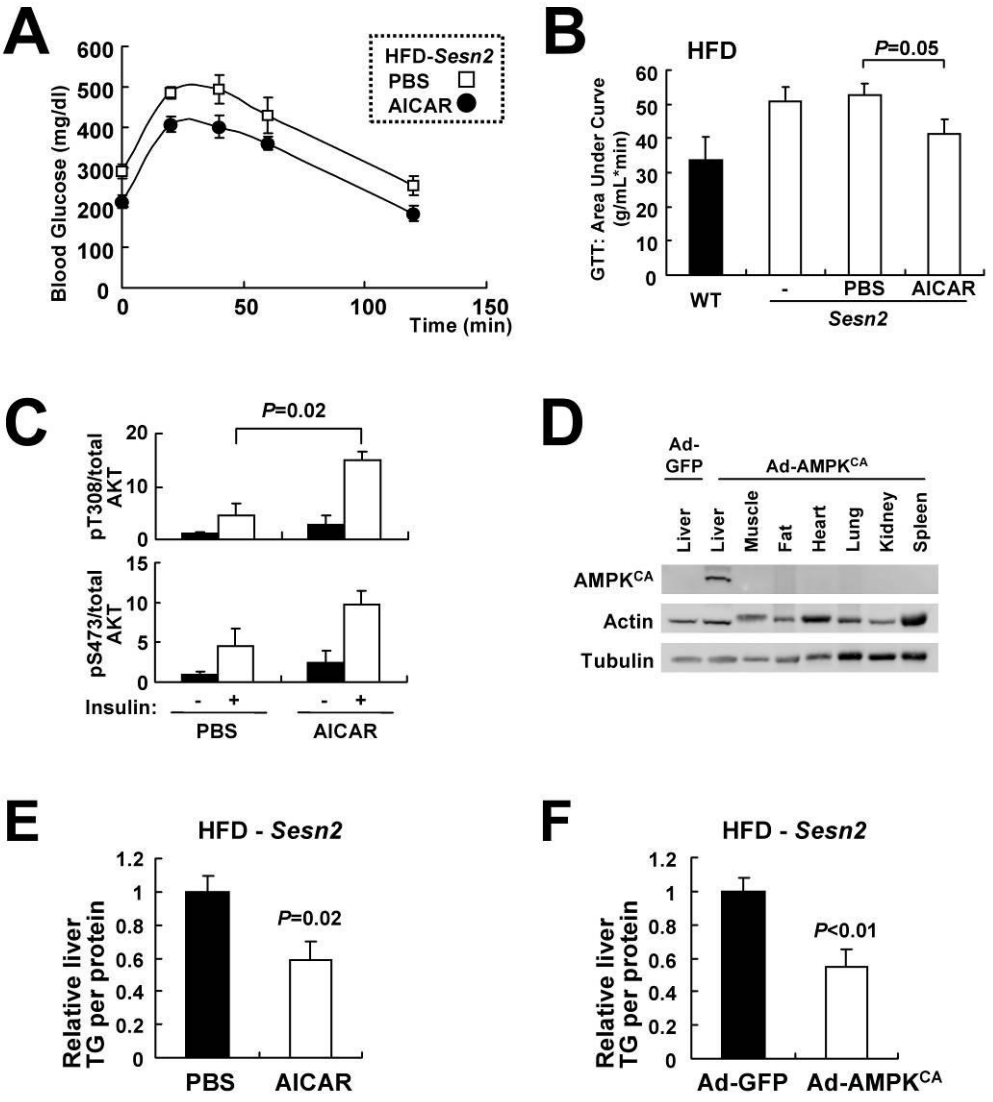
A
HFD-Sesn2
PBS
AICAR
Blood Glucose (mg/dl)
Time (min)
B
HFD
P=0.05
GTT: Area Under Curve (g/mL*min)
WT
PBS
AICAR
Sesn2
C
P=0.02
pT308/total AKT
pS473/total AKT
Insulin:
PBS
AICAR
D
Ad-GFP
Ad-AMPKCA
Liver
Muscle
Fat
Heart
Lung
Kidney
Spleen
AMPKCA
Actin
Tubulin
E
HFD - Sesn2
Relative liver TG per protein
P=0.02
PBS
AICAR
F
HFD - Sesn2
Relative liver TG per protein
P<0.01
Ad-GFP
Ad-AMPKCA

Figure S4

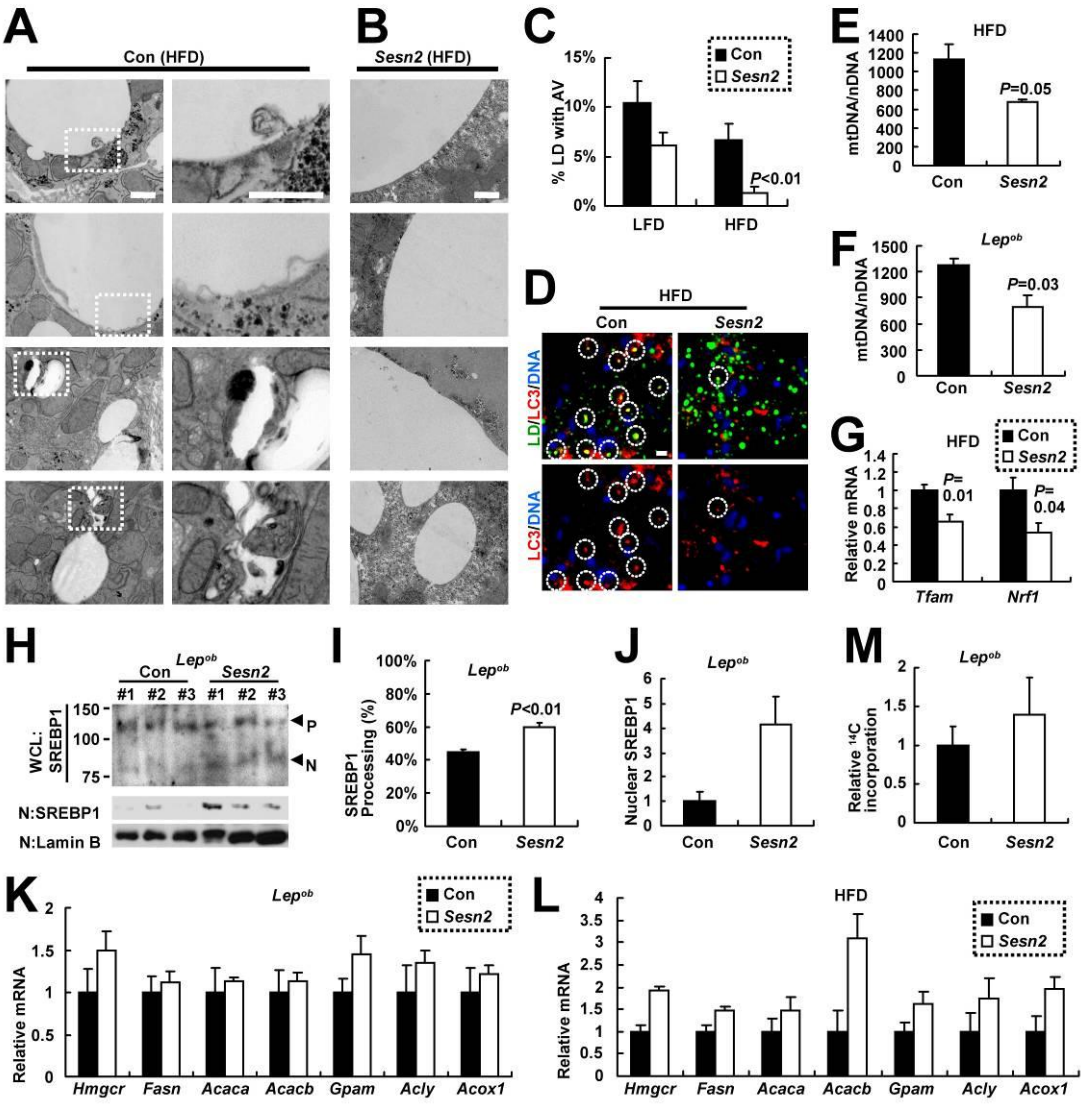
A
Con (HFD)
B
Sesn2 (HFD)
C
15%
10%
5%
0%
% LD with AV
Con
Sesn2
P<0.01
LFD
HFD
D
HFD
Con
Sesn2
LD/LC3/DNA
LC3/DNA
E
HFD
mtDNA/nDNA
1400
1200
1000
800
600
400
200
0
P=0.05
Con
Sesn2
F
Lepob
mtDNA/nDNA
1500
1200
900
600
300
0
P=0.03
Con
Sesn2
G
HFD
Con
Sesn2
Relative mRNA
1.4
1.2
1
0.8
0.6
0.4
0.2
0
P= 0.01
P= 0.04
Tfam
Nrf1
H
Lepob
Con
Sesn2
#1 #2 #3 #1 #2 #3
WCL: SREBP1
150
100
75
P
N
N:SREBP1
N:Lamin B
I
Lepob
SREBP1 Processing (%)
100%
80%
60%
40%
20%
0%
P<0.01
Con
Sesn2
J
Lepob
Nuclear SREBP1
6
5
4
3
2
1
0
Con
Sesn2
M
Lepob
Relative 14C incorporation
2
1.5
1
0.5
0
Con
Sesn2
K
Lepob
Con
Sesn2
Relative mRNA
2
1.5
1
0.5
0
Hmgcr
Fasn
Acaca
Acacb
Gpam
Acly
Acox1
L
HFD
Con
Sesn2
Relative mRNA
4
3.5
3
2.5
2
1.5
1
0.5
0
Hmgcr
Fasn
Acaca
Acacb
Gpam
Acly
Acox1

Figure S5

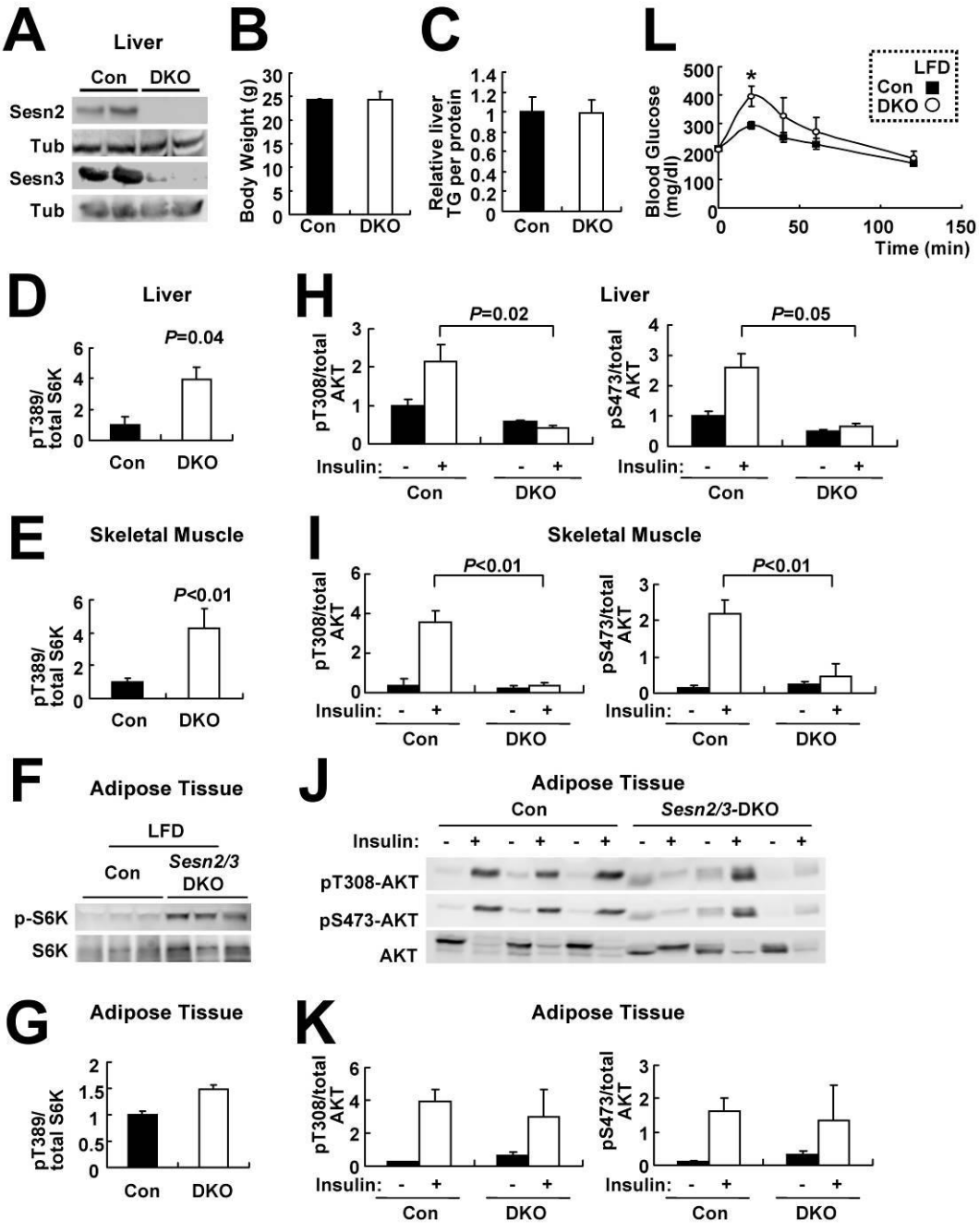
A
Liver
Con
DKO
Sesn2
Tub
Sesn3
Tub
B
Body Weight (g)
Con
DKO
C
Relative liver TG per protein
Con
DKO
L
Blood Glucose (mg/dl)
Time (min)
LFD
Con
DKO
D
Liver
P=0.04
pT389/ total S6K
Con
DKO
H
Liver
P=0.02
pT308/total AKT
Insulin:
Con
DKO
P=0.05
pS473/total AKT
Insulin:
Con
DKO
E
Skeletal Muscle
P<0.01
pT389/ total S6K
Con
DKO
I
Skeletal Muscle
P<0.01
pT308/total AKT
Insulin:
Con
DKO
P<0.01
pS473/total AKT
Insulin:
Con
DKO
F
Adipose Tissue
LFD
Con
Sesn2/3 DKO
p-S6K
S6K
J
Adipose Tissue
Con
Sesn2/3-DKO
Insulin:
pT308-AKT
pS473-AKT
AKT
G
Adipose Tissue
pT389/ total S6K
Con
DKO
K
Adipose Tissue
pT308/total AKT
Insulin:
Con
DKO
pS473/total AKT
Insulin:
Con
DKO

Figure S6

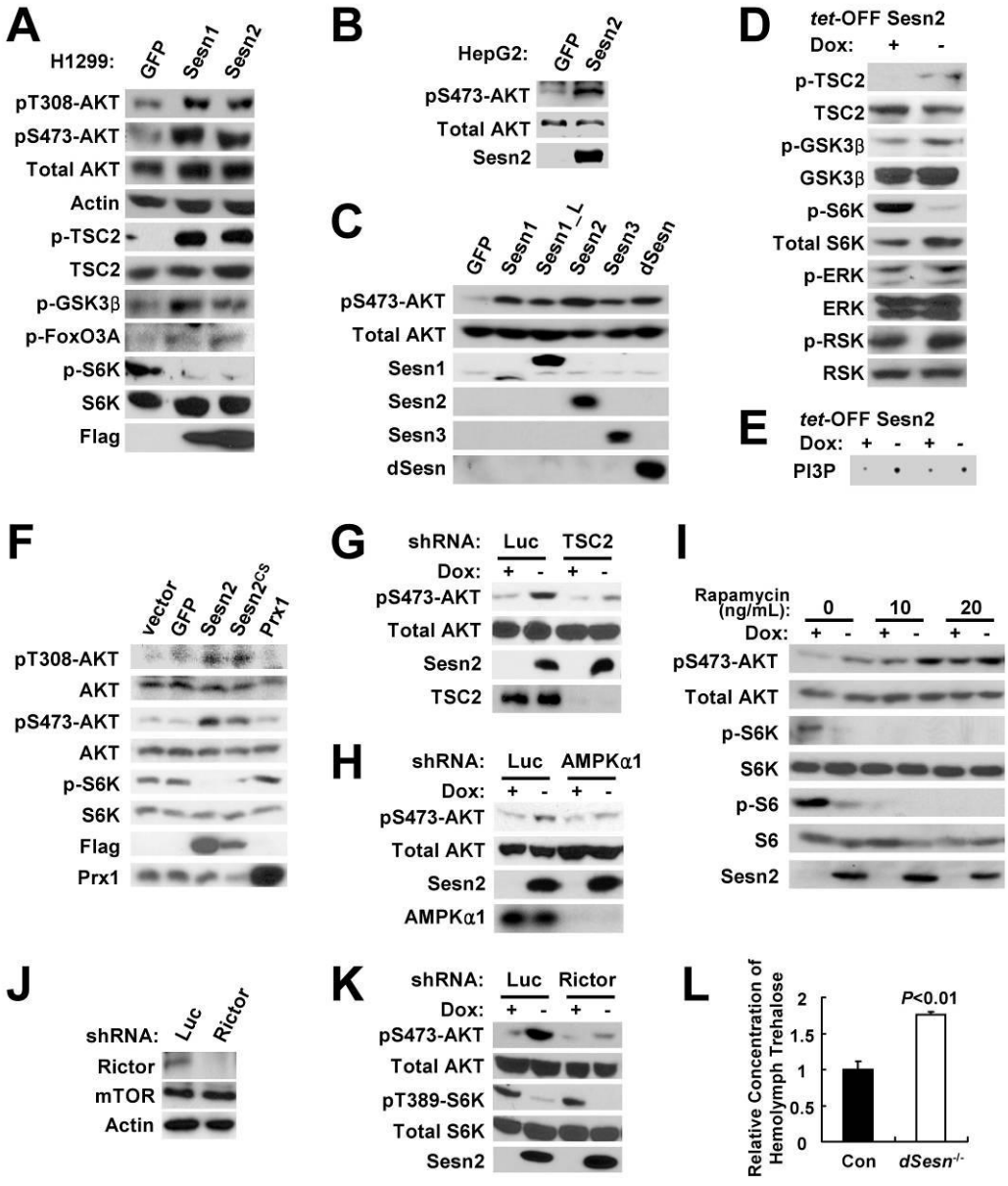
A
H1299:
GFP
Sesn1
Sesn2
pT308-AKT
pS473-AKT
Total AKT
Actin
p-TSC2
TSC2
p-GSK3β
p-FoxO3A
p-S6K
S6K
Flag
B
HepG2:
GFP
Sesn2
pS473-AKT
Total AKT
Sesn2
C
GFP
Sesn1
Sesn1_L
Sesn2
Sesn3
dSesn
pS473-AKT
Total AKT
Sesn1
Sesn2
Sesn3
dSesn
D
tet-OFF Sesn2
Dox: + -
p-TSC2
TSC2
p-GSK3β
GSK3β
p-S6K
Total S6K
p-ERK
ERK
p-RSK
RSK
E
tet-OFF Sesn2
Dox: + - + -
PI3P
F
Vector
GFP
Sesn2
Sesn2CS
Prx1
pT308-AKT
AKT
pS473-AKT
AKT
p-S6K
S6K
Flag
Prx1
G
shRNA: Luc TSC2
Dox: + - + -
pS473-AKT
Total AKT
Sesn2
TSC2
H
shRNA: Luc AMPKα1
Dox: + - + -
pS473-AKT
Total AKT
Sesn2
AMPKα1
I
Rapamycin (ng/mL): 0 10 20
Dox: + - + - + -
pS473-AKT
Total AKT
p-S6K
S6K
p-S6
S6
Sesn2
J
shRNA: Luc Rictor
Rictor
mTOR
Actin
K
shRNA: Luc Rictor
Dox: + - + -
pS473-AKT
Total AKT
pT389-S6K
Total S6K
Sesn2
L
Relative Concentration of Hemolymph Trehalose
2
1.5
1
0.5
0
P<0.01
Con
dSesn-/-

Figure S7

Supplemental Figure Legends

Figure S1. Phenotypes of *Sesn2*$^{-/-}$ mice, related to Figure 1.

(A-C) Normal physiological phenotypes of *Sesn2*$^{-/-}$ mice kept on LFD. (A) Body weight of Con (*Sesn2*$^{+/+}$ or *Sesn2*$^{+/-}$, black bars) and *Sesn2*$^{-/-}$ (white bars) mice of the indicated ages (mo) kept on LFD (n≥9). (B) Normal glucose tolerance in *Sesn2*$^{-/-}$ mice kept on LFD. After 6 hrs of fasting, 6 month-old Con (n=17, closed square) and *Sesn2*$^{-/-}$ (n=13, open circle) mice kept on LFD were subjected to glucose tolerance tests (GTT). (C) Normal insulin tolerance of *Sesn2*$^{-/-}$ mice kept on LFD. After 6 hrs of fasting, 6 month-old Con (n=17, closed square) and *Sesn2*$^{-/-}$ (n=13, open circle) mice kept on LFD were subjected to insulin tolerance tests (ITT). (D-I) Sestrin2 expression is induced upon HFD-induced obesity. (D) Amounts of Sestrin1 (*Sesn1*), Sestrin2 (*Sesn2*) and Sestrin3 (*Sesn3*) mRNAs were measured in livers of 4 month-old wild-type mice kept on LFD or HFD for 2 months, using quantitative reverse transcriptase-real time PCR (RT-PCR, n≥7). (E and F) Amounts of Sestrins and tubulin were measured by immunoblotting in livers of 4-month-old WT (*Sesn2*$^{+/+}$) or *Sesn2*$^{-/-}$ mice kept on LFD or on HFD for 2 months (E). Ratio of Sestrin2 to tubulin was quantified from livers of wild-type mice on LFD or HFD (n=5), and presented as a bar graph (F). (G) Amounts of Sestrins and tubulin were measured in liver, muscle and adipose tissues of 6-month-old control (*Sesn2*$^{+/-}$) or *Sesn2*$^{-/-}$ mice kept on LFD or on HFD for 4 months, by immunoblotting (n=3). The liver cell lysates are same as in Figure 3A. (H and I) Relative mRNA amounts of Sestrin1 (*Sesn1*), Sestrin2 (*Sesn2*) and Sestrin3 (*Sesn3*) were quantified in livers of Con and *Sesn2*$^{-/-}$ mice kept on HFD (H), or *Lep*$^{ob/ob}$/*Sesn2*$^{+/-}$ and *Lep*$^{ob/ob}$/*Sesn2*$^{-/-}$ mice kept on LFD (I), using quantitative RT-PCR (n=4). (J-P) Sestrin2 deficiency does not affect the development of obesity. (J) Weight gain of Con (*Sesn2*$^{+/+}$ or

Sesn2$^{+/-}$ littermates) and *Sesn2*$^{-/-}$ mice (n≥25), which were kept on LFD until 6 to 8 weeks of age (week 0) and then maintained on HFD for the indicated times. (K) Daily food consumption of Con and *Sesn2*$^{-/-}$ mice kept on HFD for 4 months (n=8). (L) Serum insulin levels of Con and *Sesn2*$^{-/-}$ mice kept on HFD for 3 months were measured at the indicated time points during GTT (n=5). (M and N) Body weight (M) and daily food consumption (N) of Con (*Lep*$^{ob/ob}$/*Sesn2*$^{+/-}$) or *Sesn2* (*Lep*$^{ob/ob}$/*Sesn2*$^{-/-}$) mice at 4 months age (n≥4). (O) Representative MRI images of Con (*Lep*$^{ob/ob}$/*Sesn2*$^{+/-}$) and *Sesn2* (*Lep*$^{ob/ob}$/*Sesn2*$^{-/-}$) mice at 4 months age visualizing subcutaneous and intra-abdominal fat pads. (P) Quantification of total (TO), subcutaneous (SC) and intra-abdominal (IA) fat volumes of Con (*Lep*$^{ob/ob}$/*Sesn2*$^{+/-}$) and *Sesn2* (*Lep*$^{ob/ob}$/*Sesn2*$^{-/-}$) mice by MRI (n=5). Data are presented as means ± standard error. *P* values were calculated using Student's t-test.

Figure S2. Insulin responsiveness of *Sesn2*$^{-/-}$ mice kept on HFD, related to Figure 2.

(A-C) Hyperinsulinemic-euglycemic clamp experiments. Serum insulin levels (A), glucose disposal rates (GDR, B), and hepatic glucose production rates (HGP, C) of Con (*Sesn2*$^{+/+}$ or *Sesn2*$^{+/-}$) and *Sesn2*$^{-/-}$ mice kept on HFD, before (Basal) and after (Clamp) insulin infusion during a hyperinsulinemic-euglycemic clamp (n≥8). (D-G) Insulin response of adipose tissue from HFD-fed *Sesn2*$^{-/-}$ mice. (D and E) % Suppression of serum free fatty acids (FFA) (D), and serum FFA levels of HFD-fed Con (*Sesn2*$^{+/+}$ or *Sesn2*$^{+/-}$) and *Sesn2*$^{-/-}$ mice before (Basal) and after (Clamp) insulin infusion (E), during hyperinsulinemic-euglycemic clamp (n≥8). (F and G) Primary adipocytes were isolated from Con and *Sesn2*$^{-/-}$ mice kept on HFD, and incubated in the presence of C^{14}-labeled 2-deoxyglucose (DOG) after mock or insulin stimulation. 2-DOG uptake was quantified by scintillation counting, and % induction of 2-DOG uptake by insulin (F) and 2-

DOG uptake before (-) and after (+) insulin treatment (G) was calculated (n=10). (H) Expression of FoxO1 target genes in livers of obese *Sesn2*$^{-/-}$ mice. Relative mRNA amounts of the indicated FoxO1 target genes were quantified in livers of Con and *Sesn2*$^{-/-}$ mice kept on HFD using quantitative RT-PCR (n=4). (I-L) Insulin-induced activation of AKT in muscle and adipose tissue of *Sesn2*$^{-/-}$ mice kept on HFD. Muscle (I and J) and adipose tissue (K and L) were collected from Con (*Sesn2*$^{+/+}$ or *Sesn2*$^{+/-}$) and *Sesn2*$^{-/-}$ mice kept on HFD, after 6 hrs of fasting, before (-) or 10 min after (+) insulin injection (0.8 U/kg body weight). Phosphorylation of AKT at Thr308 and Ser473 was analyzed by immunoblotting (I and K). Ratio of phosphorylated to total AKT was quantified by densitometry (n≥5), and presented as bar graphs (J and L). Data are presented as means ± standard error. *P* values were calculated using Student's t-test.

Figure S3. Regulation of hepatic AMPK and mTORC1 activities by Sestrin2, related to Figure 3.

(A-I) AMPK-mTORC1 signaling in livers of obese *Sesn2*$^{-/-}$ mice. (A, B and E) AMPK (A and B) and S6K (E) were immunoprecipitated (IP) from indicated mouse liver homogenates and assayed for their kinase activities on SAMS (A and B) or K9 (E) peptides using radiolabeled γ-^{32}P-ATP. Amounts of peptide-incorporated ^{32}P were quantified by scintillation counting and are presented as bar graphs along with immunoprecipated protein amounts visualized by immunoblotting (IB). Data are presented as means ± standard deviation. (C, D and F-I) Phosphorylation of acetyl CoA carboxylase (ACC, C), mTOR (D), and IRS-1 (F-I) in liver lysates of indicated mice was analyzed by immunoblotting, quantified by densitometry and normalized to total proteins, and presented as bar graphs (n≥4). Immunoblots for phosphorylated proteins along with total amounts of each protein are shown for three mice of each group. All Con and *Sesn2* bands are

from a same gel image of corresponding immunoblots. (J and K) Activities of AMPK and S6K in lean *Sesn2*$^{+/-}$ and *Sesn2*$^{-/-}$ mouse livers. AMPK (J) and S6K (K) were immunoprecipitated from indicated mouse liver homogenates and assayed for their kinase activity on SAMS (J) or K9 (K) peptides using radiolabeled γ-^{32}P-ATP. Amounts of peptide-incorporated ^{32}P were quantified by scintillation counting and are presented as bar graphs along with immunoprecipated total protein visualized by immunoblotting. Relative AMPK and S6K activities were normalized to the immunoprecipitated total protein amount (left panels, n=3). Data are presented as means ± standard error (left panels) or standard deviation (right panels). (L and M) Insulin-induced AKT phosphorylation in liver and adipose tissue of lean *Sesn2*$^{+/-}$ and *Sesn2*$^{-/-}$ mice. Livers (L) and adipose tissues (M) were collected from Con and *Sesn2*$^{-/-}$ mice kept on LFD, after 6 hrs of fasting, before (-) or 10 min after (+) insulin injection (0.8U/kg body weight). Phosphorylations of AKT at Thr308 and Ser473 were analyzed by immunoblotting (upper panels). Ratio of phosphorylated to total AKT was determined by densitometry (n≥5, lower panels). Unless indicated, data are presented as means ± standard error. *P* values were calculated using Student's t-test.

Figure S4. Hepatic AMPK reactivation restores glucose and lipid homeostasis in HFD-fed *Sesn2*$^{-/-}$ mice, related to Figure 4.

(A) *Sesn2*$^{-/-}$ mice kept on HFD for 3 months were subjected to daily injection of 250 mg/kg body weight AICAR or vehicle (PBS) for 7 days. After 6 hrs of fasting, the mice were subjected to GTT (n≥5). (B) Area-under-curve analysis of GTT (A) data. Values from untreated *Sesn2*$^{+/+}$ (WT) and *Sesn2*$^{-/-}$ (-) mice kept on the same HFD protocol were provided as reference. (C) After 10 days of AICAR or vehicle (PBS) injection, livers from the mice described above were collected after 6 hrs of fasting, before (-) or 10 min after (+) insulin injection (0.8 U/kg body

weight). The livers were analyzed for phosphorylation and expression of AKT as in Figure 4C. Ratios of phosphorylated to total AKT were determined by densitometry (n=3). (D) Immunoblot analysis of myc-tagged $AMPK^{CA}$ expression in indicated tissues of mice infected with Ad-GFP or Ad-$AMPK^{CA}$. Tubulin and actin were used as loading controls. (E and F) Relative liver triglycerides (TG) per protein were measured in *Sesn2*$^{-/-}$ mice kept on HFD, treated with vehicle (PBS) or 250 mg/kg/day AICAR for 10 days (E), or 96 hrs after infection with Ad-GFP or Ad-$AMPK^{CA}$ (F), and presented as bar graphs (n≥5). Data are presented as means ± standard error. *P* values were calculated using Student's t-test.

Figure S5. Aggravation of HFD-induced hepatosteatosis by Sestrin2 loss, related to Figure 5. (A-D) Autophagic activity associated with LD is diminished in *Sesn2*$^{-/-}$ mice kept on HFD. (A and B) Electron micrographs of livers from control (A) and *Sesn2*$^{-/-}$ (B) mice kept on HFD. Autophagic vesicles (AV) associated with lipid droplets (LD) in control livers (A, dotted boxes in the left panels) were magnified in the right panels. Such vesicles were hardly found in *Sesn2*$^{-/-}$ livers (B). Scale bars: 1 μm. (C and D) Defective LD autophagy in *Sesn2*$^{-/-}$ liver of obese mice. (C) Quantification of the association between LD and AV from EM images (n≥8). (D) LD, AV, and DNA were visualized in frozen liver sections of the indicated mice with BODIPY 493/503 (green), anti-LC3 antibody (red), and DAPI (blue), respectively. Scale bar, 5 μm. Dotted circles indicate LDs associated with prominent amount of LC3. (E-G) Sestrin2 loss decreased mitochondrial amount and reduced expression of mitochondrial biogenesis marker genes in liver. (E and F) Ratio of mitochondrial DNA (mtDNA) to nuclear DNA (nDNA) in livers of the indicated mice (n≥3) was determined by quantitative real time PCR of *Nd1* and *Lpl*, respectively. (G) Relative amounts of the indicated mRNAs were measured in livers of Con and *Sesn2*$^{-/-}$ mice

kept on HFD (n=5) by quantitative RT-PCR. (H-M) Lipogenesis activities in *Lep*$^{ob/ob}$/*Sesn2*$^{+/-}$ and *Lep*$^{ob/ob}$/*Sesn2*$^{-/-}$ livers. (H) Unprocessed (P, ~125kDa) and processed (N, ~68kDa) SREBP1 amounts were examined by immunoblot analyses of whole liver lysates (WCL) of *Lep*$^{ob/ob}$/*Sesn2*$^{+/-}$ (Con) or *Lep*$^{ob/ob}$/*Sesn2*$^{-/-}$ (*Sesn2*). Nuclear extracts (N) were prepared from frozen livers of *Lep*$^{ob/ob}$/*Sesn2*$^{+/-}$ (Con) or *Lep*$^{ob/ob}$/*Sesn2*$^{-/-}$ (*Sesn2*) mice and analyzed for SREBP1 and Lamin B1 expression. (I) Ratio of processed to total SREBP1 was quantified by densitometry and presented as a bar graph (n≥4). (J) Ratio of nuclear SREBP1 to Lamin B1 was quantified by densitometry and presented as a bar graph (n≥4). (K and L) Relative amounts of lipogenic mRNAs were determined in livers of *Lep*$^{ob/ob}$/*Sesn2*$^{+/-}$ and *Lep*$^{ob/ob}$/*Sesn2*$^{-/-}$ mice (K), or Con (*Sesn2*$^{+/+}$ and *Sesn2*$^{+/-}$) and *Sesn2*$^{-/-}$ mice kept on HFD (L) by quantitative RT-PCR (n=4). (M) Lipogenesis was measured by 1,2-^{14}C-acetate incorporation into liver slices from *Lep*$^{ob/ob}$/*Sesn2*$^{+/-}$ (Con) or *Lep*$^{ob/ob}$/*Sesn2*$^{-/-}$ (*Sesn2*) mice, and presented as a bar graph (n=3). Data are presented as means ± standard error. *P* values were calculated using Student's t-test.

Figure S6. Phenotypes of Sestrin2/3-double knockout mice, related to Figure 6.

(A) Livers of 4 months-old *Sesn2*$^{+/-}$ (Con) and *Sesn2*$^{-/-}$/*Sesn3*$^{-/-}$ (DKO) mice kept on LFD were analyzed by immunoblotting for the indicated proteins. (B) Body weights of 4 months-old Con and DKO mice kept on LFD (n=3). (C) Liver triglycerides (TG) in 4 months-old Con and DKO mice kept on LFD (n=3). (D-G) *Sesn2*$^{-/-}$/*Sesn3*$^{-/-}$ (DKO) mice exhibit elevated mTORC1-dependent S6K phosphorylation. Livers (D), skeletal muscles (E), and adipose tissues (F and G) of 4 months-old Con (*Sesn2*$^{+/-}$) and DKO mice kept on LFD were homogenized and analyzed by immunoblotting for S6K phosphorylation on Thr389. Ratio of phosphorylated to total S6K was determined by densitometry (n=3). (H-K) Livers (H), skeletal muscles (I) and adipose tissues (J

and K) were collected from Con and DKO mice, after 6 hrs of fasting, before (-) or 10 min after (+) insulin injection (0.8 U/kg body weight), homogenized and analyzed by immunoblotting with indicated antibodies. Ratios of phosphorylated to total AKT were quantified by densitometry, and presented as bar graphs (n=3). (L) After 6 hrs of fasting, 4 month-old Con and DKO mice kept on LFD were subjected to GTT (n=3). Star (*) denotes P=0.05. Data are presented as means ± standard error. P values were calculated using Student's t-test.

Figure S7. Sestrins activate AKT signaling, related to Figure 7.

(A-C) Activation of AKT by Sestrin homologues. H1299 (A and C) and HepG2 (B) cells were infected with lentiviral vectors encoding GFP, Sestrin1 (Sesn1), long isoform of Sestrin1 (Sesn1-L), Sestrin2 (Sesn2), Sestrin3 (Sesn3) and dSestrin. Sestrins were tagged with HA, Flag or Myc epitopes. Protein phosphorylation and expression were examined at 48 hrs post infection by immunoblotting. (D) Phosphorylation of AKT downstream targets, TSC2 at Thr1462 and GSK3β at Ser9, is enhanced upon Sestrin2 expression. Phosphorylation of S6K was silenced while phosphorylation of ERK and RSK was not altered by Sestrin2 induction. The cell lysates are the same as in Figure 7C and protein phosphorylation and expression were analyzed by immunoblotting. (E) Activation of PI3K upon Sestrin2 expression. Flag-tagged Sestrin2 was induced in MCF7-tet OFF Sesn2F cells by doxycycline (Dox) removal (-). Control cultures were left with Dox (+). PI3K activity was assayed after 24 hrs and phosphorylated lipid substrates (PI3P) were visualized after a thin layer chromatography-autoradiography. (F) Activation of AKT by Sestrin2 does not depend on its redox activity. H1299 cells were infected with lentiviral vectors encoding WT, redox-inactive (CS) Sestrin2, and Prx1. Controls were infected with either empty or a GFP lentivirus. Sestrins were tagged with Flag epitope. Protein phosphorylation and

expression were examined at 48 hrs post infection by immunoblotting. (G and H) Sestrin2 activation of AKT is TSC2 and AMPK dependent. MCF7-tet OFF Sesn2F cells were infected with sh-TSC2, sh-AMPKα1 or sh-Luc lentiviruses. After 48 hrs, Sestrin2 was induced by doxycycline removal and protein phosphorylation and expression were examined 24 hrs later. (I) Inhibition of mTORC1 by rapamycin treatment can provoke AKT activation as effectively as Sestrin2 induction. In MCF7-tet OFF Sesn2F cells, Sestrin2 was induced by doxycycline removal. After 24 hrs, rapamycin was added at the indicated concentrations, and protein phosphorylation and expression were examined 30 min later. (J and K) Sestrin activation of AKT is dependent on mTORC2. MCF7 (J) or MCF7-tet OFF Sesn2F (K) cells were infected with sh-Rictor or sh-Luc lentiviruses. Silencing efficiency for Rictor was measured at 48 hrs after infection (J). For Sestrin2 induction, doxycycline was removed after 48 hrs of lentiviral infection, and protein phosphorylation and expression were examined 24 hrs later (K). (L) *Drosophila* Sestrin controls AKT signaling and blood sugar level. Relative hemolymph trehalose concentrations were measured in thirty control (w^{1118}) and $dSesn^{-/-}$ ($dSesn^{\Delta 11}$) adult male flies, and presented as a bar graph. Error bars indicate standard deviation (n=3). *P* value was calculated using Student's t-test.

Supplemental Experimental Procedures

Genotyping

Genomic DNA was extracted from tissues or tails by proteinase K digestion (proteinase K 0.5 mg/mL, 100 mM Tris HCl [pH 8.5], 200 mM NaCl, 5 mM EDTA, 0.2% SDS) followed by phenol chloroform extraction and ethanol precipitation. The following primers were used for *Sesn2* genotyping: forward 5'-CTTGGGAGTTCATCTAGATTAG-3'; reverse WT 5'-GCTAAGTGGTCGGATGATAG-3'; reverse *Sesn2* 5'-CACTCCAAACTCCGCAAACTC-3'. *Lep*^{ob} genotyping was done as described (Namae et al., 1998). The following primers were used for *Sesn3* genotyping: forward 5'-ACAGTGGGCTCCATTCTCAG-3'; reverse 5'-GCCATGTGCCATGTAACAAC-3'.

Immunoblotting and Immune Complex Kinase Assays

For ordinary immunoblot analysis, cells and tissues were lysed in RIPA-SDS buffer (Budanov and Karin, 2008) or cell lysis buffer (Lee et al., 2010). For cell fractionation studies, Nuclear Extract Kit (Active Motif) was used according to manufacturer's instruction. Proteins were resolved by SDS-PAGE, transferred onto PVDF membranes and probed with the relevant antibodies. Chemiluminescence was detected using X-ray film (Phenix), Versadoc (Bio-rad), or LAS4000 (GE) systems. For immunoprecipitation kinase assays, tissues were lysed in cell lysis buffer plus protease inhibitor cocktail (Lee et al., 2010). Cleared lysates were incubated with AMPK or S6K antibodies for 3 hrs followed by incubation with protein A/G beads. The AMPK assay was performed as described (Hardie et al., 2000) in the presence of 2 mM AMP and using SAMS peptide (Biomol) as a substrate. The S6K assay was performed with K9 (KKRNRTLTK)

peptide substrate using a p70 S6 kinase assay kit (Upstate), according to manufacturer's recommendation. The phosphorylated peptides were bound to P81 membrane and incorporated radioactivity was quantified by liquid scintillation counting (Lee et al., 2007). The PI3K assay was performed as described (Wang and Summers, 2003) using anti-phosphotyrosine antibodies.

Lipid Metabolism Assays

Liver triglycerides were extracted in chloroform/methanol (2:1, v/v) and were measured using Triglyceride-SL assay kit (Genzyme Diagnotics) according to manufacturer's instructions as described (Lee et al., 2010; Park et al., 2010). For relative measurement, triglycerides were extracted in 10% NP-40 solution. The triglyceride readings were normalized to protein amounts measured by the Bio-Rad protein assay kit (Bio-rad). β-oxidation was measured using liver homogenates and ^{14}C-labeled palmitate, as described (Bandyopadhyay et al., 2006). For lipogenesis assay, liver samples were sliced and taken into 0.2 mL Hepes-Salt-buffer containing 0.5% fatty acid free BSA and 1mM unlabelled sodium acetate in 2 mL tubes. Then, 2 μCi of 1,2-^{14}C-acetate was added to each tube and incubated for 60 min at 37^{o}C. Incubations were terminated by homogenizing after adding 0.1 mL 1N HCl to each tube followed by the addition of 0.7 mL of a mixture of chloroform and methanol (2:1, v/v). The tubes were vortexed and centrifuged to separate two layers. The lower chloroform layers were collected, evaporated and counted for incorporation of ^{14}C-labeled acetate into lipids. An aliquot of the homogenates was saved for protein assay before adding organic solvent.

RNA Analysis

Total RNA was isolated from tissues or cells using Trizol (Invitrogen), and cDNA was

made using MMLV-RT (Promega) with random hexamers (Invitrogen). Relative transcript amounts were measured by an iCycler iQ Real-Time PCR system (Bio-rad) using relevant primers (see below), and normalized to the amount of cyclophilin or ribosomal protein S3 mRNA. Northern blot was done as described (Budanov et al., 2004).

Urine Glucose Quantification

For urine glucose measurement, reads on a one-touch ultra glucose meter from 2 month-old C57BL/6 mice urine (standard urine), which does not contain significant amount of glucose (Wade et al., 2008), were set as blank. Glucose was dissolved in standard urine to generate standard curve for the glucose meter to estimate the urine glucose level. 0 mg/dl to 180 mg/dl glucose in urine can be measured using this method. If the glucose meter gave a higher value, a serial dilution in standard urine was performed to generate a readable value.

Fluorescence Staining

For fluorescence staining of LD and LC3, frozen liver sections were fixed with 2% paraformaldehyde, blocked with 1X Western Blocking Reagent (Roche), and incubated with anti-LC3B primary antibody (Cell Signaling) followed by Alexa 594-conjugated secondary antibody, DAPI and BODIPY 493/503 (Invitrogen). Immunostaining of *Drosophila* wing imaginal disc was done as described (Lee et al., 2010).

MRI Analysis

Mice were imaged while under ketamine anesthesia. Data were collected using a 10 cm volume wrist coil (Mayo Clinic Rochester, MN) with a clinical 3 Tesla Magnetic resonance

imaging (MRI) scanner (GE Medical Systems, Milwaukee, WI). Images were acquired using a T1-weighted pulse sequence that rendered fat bright and nonfat tissues dark. Pulse sequence: 2D spin echo sequence TE/TR = 13/500, field of view (FOV) 8 cm, phase FOV 50% with a zipped 512 x 512 matrix, slice thickness 1mm, 4 averages. This provided an in-plane resolution of 156 microns. Image data sets were segmented and volumes were rendered using Amira software (Visage Imaging Inc. San Diego CA).

Transmission Electron Microscopy

Mouse liver tissues were fixed through whole-body perfusion with fixation buffer composed of 2% paraformaldehyde and 2.5% glutaraldehyde (Ted Pella, Redding, CA) in 0.1 M sodium cacodylate buffer (pH 7.4). Dissected pieces of mouse liver were placed in fixation buffer on ice for 1 hr. The samples were washed three times with buffer consisting of 0.1 M sodium cacodylate plus 3 mM calcium chloride (pH 7.4) on ice and then post-fixed with 1% osmium tetroxide, 0.8% potassium ferrocyanide, 3 mM calcium chloride in 0.1 M sodium cacodylate (pH 7.4) for 1 hr, washed three times with ice-cold distilled water, en bloc stained with 2% uranyl acetate at 4°C for 1 hr, dehydrated through graded ethanol solutions, and embedded in Durcupan ACM resin (Fluka, St. Louis, MO). Ultrathin (80 nm) sections were post-stained with uranyl acetate and lead salts prior to imaging using a JEOL 1200FX transmission EM operated at 80 kV. Images were shot at a magnification of 2000 and digitized at 1800 dpi using a Nikon CoolScan system, giving an image size of 4033 x 6010 pixels and a pixel resolution of 5.3 nm. Lipid droplet sizes, autophagic activities, and mitochondrial amounts were quantified in a blinded manner.

Trehalose Quantification

For trehalose quantification of *Drosophila* hemolymph, a previously described protocol (Isabel et al., 2005) was modified as follows: 30 flies were homogenized in 500 μL of 70% ethanol. 150 μL aliquots of cleared homogenate were lyophilized and dissolved in 200 μL of 2% NaOH and incubated at 100°C for 10 min to destroy reducing sugars, after which the tubes were rapidly cooled in ice-cold water. The nonreducing trehalose was subsequently quantified by adding 1.5 mL cold freshly prepared anthrone reagent. Trehalose standards were dissolved in 70% ethanol and subjected to the same protocol as the *Drosophila* samples.

Fly Strains

w^{1118}, *ap-GAL4*, *UAS-dSesn*^{WT} (*dSesn*^{XP4}), *UAS-dSesn*^{CS}, *UAS-Rheb*, *UAS-S6K*^{CA}, *dSesn*^{8A11} strains were described (Lee et al., 2010). *UAS-siAMPK* was from the Bloomington stock center.

Antibodies

Sestrin1 antibodies were generated from GST-Sestrin1 fusion protein as described (Lee et al., 2010). Sestrin2 (Proteintech), Sestrin3 (Abcam), *Drosophila* Sestrin (Lee et al., 2010), phospho-Thr308-AKT (Cell Signaling), phospho-Ser473-AKT (Cell Signaling), Actin (Amersham), p53 (Santa Cruz), phospho-Thr172-AMPK (Abgent), AMPK-α1/2 (Santa Cruz), pSer79-ACC (Cell Signaling), ACC (Upstate), phospho-Ser2481-mTOR (Cell Signaling), mTOR (Cell Signaling), S6K (Santa Cruz), IRS-1 (Upstate), phospho-Ser636-IRS (Santa Cruz), phospho-Ser639-IRS (Santa Cruz), phospho-Ser641-IRS (Santa Cruz), phospho-Tyr1229-IRS (Santa Cruz), SREBP1 (Santa Cruz), phospho-Ser256-FoxO1 (Cell Signaling), FoxO1 (Cell

Signaling), Tubulin (Sigma), AMPK-α1 (Santa Cruz), Lamin B1 (Santa Cruz), phospho-Thr1462-TSC2 (Cell Signaling), TSC2 (Cell Signaling), phospho-Ser9-GSK3β (Cell Signaling), phospho-ERK (Cell Signaling), ERK (Cell Signaling), phospho-RSK (Cell Signaling), RSK (Cell Signaling), phospho-Thr389-S6K (Cell Signaling), phospho-Ser411-S6K (Santa Cruz), LC3B (Cell Signaling), Flag (Sigma), Myc (Santa Cruz), HA (Roche), Wingless (Developemental Studies Hybridoma Bank), and phospho-Ser505-*Drosophila*-AKT (Cell Signaling) antibodies were used for immunoblot, immunoprecipitation and immunostaining experiments.

shRNA-mediated Gene Silencing

shRNA-mediated gene silencing was done using a lentiviral system as described (Budanov and Karin, 2008). sh-Luc, sh-TSC2, sh-AMPKα1 (Budanov and Karin, 2008), sh-p53 (Sablina et al., 2005) and sh-c/EBPβ (Gomis et al., 2006) constructs were described.

Adenoviral Procedures

Ad-GFP and Ad-AMPK^{CA} vectors were previously described (Foretz et al., 2005; Luo et al., 2007). For hepatic gene transduction, 10^9 pfu of adenoviruses were injected through the tail vein.

Primers

Cyclophillin (Solinas et al., 2007), *Ribosomal Protein S3* (Oh et al., 2010), *Sesn1, Sesn2, Sesn3* (Chen et al., 2010), *Hmgcr*, *Gpam*, *Acly*, *Acox1* (Zhang et al., 2006), *Pepck1*, *Fasn*, *Acaca*, *Acacb* (Grefhorst et al., 2005) primers were designed as previously described. *Tfam* (forward: 5'-

CCCAAATTTAAAGCTAAACACCCAGATGC-3', reverse: 5'-CCCATCAGCTGACTTGGA GTTAGC-3') and *Nrf1* (forward: 5'-GGCTGCTGCAGGTCCTGTGGG-3', reverse: 5'-GGTGCTGCGCCAAACACC-3') primers were used as mitochondrial biogenesis markers. Mitochondrial DNA determination was done as described using NADH dehydrogenase (*Nd1*) and Lipoprotein lipase (*Lpl*) primers (Medeiros, 2008).

Supplemental References

Bandyopadhyay, G.K., Yu, J.G., Ofrecio, J., and Olefsky, J.M. (2006). Increased malonyl-CoA levels in muscle from obese and type 2 diabetic subjects lead to decreased fatty acid oxidation and increased lipogenesis; thiazolidinedione treatment reverses these defects. Diabetes *55*, 2277-2285.

Budanov, A.V., Sablina, A.A., Feinstein, E., Koonin, E.V., and Chumakov, P.M. (2004). Regeneration of peroxiredoxins by p53-regulated sestrins, homologs of bacterial AhpD. Science *304*, 596-600.

Budanov, A.V., and Karin, M. (2008). p53 target genes sestrin1 and sestrin2 connect genotoxic stress and mTOR signaling. Cell *134*, 451-460.

Chen, C.C., Jeon, S.M., Bhaskar, P.T., Nogueira, V., Sundararajan, D., Tonic, I., Park, Y., and Hay, N. (2010). FoxOs inhibit mTORC1 and activate Akt by inducing the expression of Sestrin3 and Rictor. Dev Cell *18*, 592-604.

Foretz, M., Ancellin, N., Andreelli, F., Saintillan, Y., Grondin, P., Kahn, A., Thorens, B., Vaulont, S., and Viollet, B. (2005). Short-term overexpression of a constitutively active form of AMP-activated protein kinase in the liver leads to mild hypoglycemia and fatty liver. Diabetes *54*, 1331-1339.

Gomis, R.R., Alarcon, C., Nadal, C., Van Poznak, C., and Massague, J. (2006). C/EBPbeta at the core of the TGFbeta cytostatic response and its evasion in metastatic breast cancer cells. Cancer Cell *10*, 203-214.

Grefhorst, A., van Dijk, T.H., Hammer, A., van der Sluijs, F.H., Havinga, R., Havekes, L.M., Romijn, J.A., Groot, P.H., Reijngoud, D.J., and Kuipers, F. (2005). Differential effects of pharmacological liver X receptor activation on hepatic and peripheral insulin sensitivity in lean and ob/ob mice. Am J Physiol Endocrinol Metab *289*, E829-838.

Hardie, D.G., Salt, I.P., and Davies, S.P. (2000). Analysis of the role of the AMP-activated protein kinase in the response to cellular stress. Methods Mol Biol *99*, 63-74.

Isabel, G., Martin, J.R., Chidami, S., Veenstra, J.A., and Rosay, P. (2005). AKH-producing neuroendocrine cell ablation decreases trehalose and induces behavioral changes in Drosophila. Am J Physiol Regul Integr Comp Physiol *288*, R531-538.

Lee, J.H., Koh, H., Kim, M., Kim, Y., Lee, S.Y., Karess, R.E., Lee, S.H., Shong, M., Kim, J.M., Kim, J.*, et al.* (2007). Energy-dependent regulation of cell structure by AMP-activated protein kinase. Nature *447*, 1017-1020.

Lee, J.H., Budanov, A.V., Park, E.J., Birse, R., Kim, T.E., Perkins, G.A., Ocorr, K., Ellisman, M.H., Bodmer, R., Bier, E.*, et al.* (2010). Sestrin as a feedback inhibitor of TOR that prevents age-related pathologies. Science *327*, 1223-1228.

Luo, J., Deng, Z.L., Luo, X., Tang, N., Song, W.X., Chen, J., Sharff, K.A., Luu, H.H., Haydon, R.C., Kinzler, K.W.*, et al.* (2007). A protocol for rapid generation of recombinant adenoviruses using the AdEasy system. Nat Protoc *2*, 1236-1247.

Medeiros, D.M. (2008). Assessing mitochondria biogenesis. Methods *46*, 288-294.

Namae, M., Mori, Y., Yasuda, K., Kadowaki, T., Kanazawa, Y., and Komeda, K. (1998). New method for genotyping the mouse Lep(ob) mutation, using a polymerase chain reaction assay. Lab Anim Sci *48*, 103-104.

Oh, D.Y., Talukdar, S., Bae, E.J., Imamura, T., Morinaga, H., Fan, W., Li, P., Lu, W.J., Watkins, S.M., and Olefsky, J.M. (2010). GPR120 is an omega-3 fatty acid receptor mediating potent anti-inflammatory and insulin-sensitizing effects. Cell *142*, 687-698.

Park, E.J., Lee, J.H., Yu, G., He, G., Ali, S.R., Holzer, R.G., Osterreicher, C.H., Takahashi, H., and Karin, M. (2010). Dietary and genetic obesity promote liver inflammation and tumorigenesis by enhancing IL-6 and TNF expression. Cell *140*, 197-208.

Sablina, A.A., Budanov, A.V., Ilyinskaya, G.V., Agapova, L.S., Kravchenko, J.E., and Chumakov, P.M. (2005). The antioxidant function of the p53 tumor suppressor. Nat Med *11*, 1306-1313.

Solinas, G., Vilcu, C., Neels, J.G., Bandyopadhyay, G.K., Luo, J.L., Naugler, W., Grivennikov, S., Wynshaw-Boris, A., Scadeng, M., Olefsky, J.M.*, et al.* (2007). JNK1 in hematopoietically derived cells contributes to diet-induced inflammation and insulin resistance without affecting obesity. Cell Metab *6*, 386-397.

Wade, J.M., Juneja, P., MacKay, A.W., Graham, J., Havel, P.J., Tecott, L.H., and Goulding, E.H. (2008). Synergistic impairment of glucose homeostasis in ob/ob mice lacking functional serotonin 2C receptors. Endocrinology *149*, 955-961.

Wang, L.P., and Summers, S.A. (2003). Measuring insulin-stimulated phosphatidyl-inositol 3-

kinase activity. Methods Mol Med *83*, 127-136.

Zhang, W., Patil, S., Chauhan, B., Guo, S., Powell, D.R., Le, J., Klotsas, A., Matika, R., Xiao, X., Franks, R.*, et al.* (2006). FoxO1 regulates multiple metabolic pathways in the liver: effects on gluconeogenic, glycolytic, and lipogenic gene expression. J Biol Chem *281*, 10105-10117.